A combined diffuse reflectance infrared Fourier transform spectroscopy–mass spectroscopy–gas chromatography for the *operando* study of the heterogeneously catalyzed CO$_2$ hydrogenation over transition metal-based catalysts

View Online   Export Citation   CrossMark

Kun Zhao,[1,2,a] iD Jie Zhang,[1,2] iD Wen Luo,[1,2,b] iD Mo Li,[1,2] iD Emanuele Moioli,[1,2] iD Mariana Spodaryk,[1,2] and Andreas Züttel[1,2] iD

AFFILIATIONS

[1] Laboratory of Materials for Renewable Energy, Institute of Chemical Sciences and Engineering, École Polytechnique Fédérale de Lausanne (EPFL), 1951 Sion, Switzerland
[2] EMPA Material Science and Technology, 8600 Dübendorf, Switzerland

[a] Author to whom correspondence should be addressed: kun.zhao@epfl.ch
[b] wen.luo@epfl.ch

ABSTRACT

We built an inline diffuse reflectance infrared Fourier transform spectroscopy–mass spectroscopy–gas chromatography (DRIFTS–MS–GC) apparatus aiming at an *operando* mechanistic study of the heterogeneously catalyzed CO$_2$ hydrogenation reaction. The multifunctional and accurate system enabled the simultaneous utilization of IR, MS, GC, and nuclear magnetic resonance techniques in one single device to analyze the surface, gas, and liquid products formed during the reaction process. To assess the potential of the system, we compared the activity of pristine metal (Fe, Co, Ni, and Cu), metal alloy (LaNi$_4$Cu), and metal–metal oxide (Co—CoO) catalysts with respect to the interactions between gaseous CO$_2$ and the catalyst surfaces. For the quantitative comparison, the rate constants and activation energies of CO$_2$ hydrogenation were determined. The results showed a composition dependent reactivity of the metals. The metal oxide mixed with the metal is essentially important for the formation of observable of the surface species deriving from CO$_2$ adsorption and for the enhancement of the CO$_2$ conversion to CH$_4$.

Published under license by AIP Publishing. https://doi.org/10.1063/1.5144497

I. INTRODUCTION

The conversion of CO$_2$ into synthetic hydrocarbons is becoming of increasing importance due to the demand of the storage of the exponentially growing renewable and sustainable energy sources.[1–3] Multiple reaction pathways, including thermal, electrochemical, and photo(electro)chemical catalysis, have been used to successfully explore the conversion processes.[4–8] At the current state of the art, thermal catalysis is the method with the highest power density and the greatest potential for scaling up due to the high activity of the catalysts employed to this scope.[9–11] However, the efficiency and selectivity of the synthetic processes are expected to be improved through the design of highly active and selective catalysts. Recent studies reported several novel catalysts for CO$_2$ hydrogenation reactions.[12,13] Ru-, Rh-, and Pd-based catalysts were found to be especially active for the transformation of CO$_2$ to CH$_4$ through the Sabatier reaction. For this reaction, a reactor based on the selected noble metal-based catalyst can succeed in reaching 99% conversion.[14–17] However, the high cost of these elements limits the employment on a large scale. Nano-sized metals on supports reduce

the economic issues as the total load can be reduced to a few weight percentage. Yet, large loading is necessary for improving activity and selectivity.[18] Ni- and Co-based catalysts, which are less expensive, are also active and widely used for CO_2 methanation. However, these catalysts show lower yields and require higher reaction temperature compared with Ru/Al_2O_3.[19–21] Numerous alterations of the active phase, such as doping,[22] alloying,[23–25] promoting,[26,27] and nanosizing,[28,29] have been attempted to increase their activity and selectivity. Yet, there is no systematical comparison of the catalysts with different structural designs in the experiment to give instructions of the choice of specifically structured catalysts.

In order to correctly address the development of new, less expensive, and more performing catalysts, suitable integrated investigation techniques are necessary. The experimental and analytical tools are two essential aspects to be addressed. The investigation methods for the CO_2 hydrogenation studies often include spectroscopic analysis, such as diffuse infrared reflectance infrared Fourier transform spectroscopy (DRIFTS),[30–33] mass spectroscopy (MS), x-ray photoelectron spectroscopy (XPS), nuclear magnetic resonance (NMR), and gas and liquid chromatography (GC and LC, respectively). However, these detection methods are generally performed independently or *ex situ*, which leads to either inconsistent experimental conditions or incomplete information. An *operando* method facilitates the collection of coherent and complete information on the reaction in one single experiment. This consideration is the main motivation for the development of the system here described.

With regard to the selection of the catalysts, ahead of designing the new materials, a systematic understanding of the fundamental differences of the metals in the CO_2 hydrogenation reaction is of great interest and importance. Recently, our group has compared the activities of the pristine metals Fe, Co, Ni, and Cu in the Sabatier reaction.[21] The results showed that Co and Ni can convert 70% and 55% CO_2 to CH_4 at 660 K and 790 K, respectively. These two pristine metals show similar activation energies of around 75 kJ/mol. Fe converted CO_2 to CO mainly above 573 K through the reversed water gas shift reaction. Cu was inactive toward CO_2 conversion. These results are consistent with the report by Weatherbee and Bartholomew in the 1980s about the silica-supported transition metals for CO_2 hydrogenation.[34] However, in these valuable studies, no information on the binding products on the surfaces during the CO_2 conversion process is provided, leaving a critical gap in the explanation of the reaction mechanisms. Theoretical simulations that calculate the elementary steps of CO_2 adsorption and hydrogenation reactions could address this issue. However, the calculations are normally performed using specified single crystalline facets and under ideal conditions.[35] These stimulate the demand of the experimental evidence of the intermediates formed under real reaction conditions in addition to the observation of the final products.

Therefore, we built an inline analysis system consisting of a diffuse reflectance infrared Fourier transform spectroscopy (DRIFTS), a mass spectroscopy (MS), and a gas chromatography (GC) analyzer. The deionized water (DIW) bottle for nuclear magnetic resonance (NMR) analysis was an optional connection. We simplified the name as DRIFTS–MS–GC. This infrastructure enables the detection of surface, gas, and liquid products during the CO_2 hydrogenation reaction over the catalyst *operando*. The careful integration of the three instruments gathers the advantages of the variously important analytical techniques and synchronizes the coherent data, which is the main innovation in the field of scientific instruments and opens the way to the investigation of reaction pathways *operando*. To the best of our knowledge, as of today, no study reports such an integrated system in operation.

Thanks to this apparatus, we systematically investigated the catalysts in the CO_2 hydrogenation reaction. Aiming at developing new highly active and efficient catalysts, we selected the first-row group 8–11 transition metal-based catalysts and designed three different forms of these metals as representative catalysts. We began with the pristine metals, aiming at understanding the fundamental distinctions of CO_2 interaction with these pure metal surfaces. Second, considering that the activation of the CO_2 molecule is hydrogen assisted, we used an alloy form, $LaNi_4Cu$ metal hydride, which can adsorb 3.63 hydrogen atoms per formula unit,[36] in order to evaluate the effect of hydrogen pre-storage in the metals on the CO_2 hydrogenation. Based on the experiences on these pristine and alloyed metals, we examined the metal oxide effect using cobalt–cobalt oxide (Co–CoO) because the metal oxide is reported to enhance the catalytic conversion of CO_2.[37]

II. METHODS

A. Setup

The DRIFTS–MS–GC setup consists of five parts, as shown in Fig. 1: part I, a gas flow controller connected to H_2, CO_2, and He gas lines, whose flows were controlled using the mass flow controller (MFC) and Labview program; part II, a DRIFTS chamber (HVC, Harrick Scientific) integrated with a Fourier transform infrared (FTIR, Tensor 27, Bruker) spectrometer using a mercury cadmium telluride (MCT) detector; part III, a mass spectrometer (MS, Pfeiffer OmniStar 320) using a detector of a Faraday cup; part IV, a sealed bottle containing DIW for the collection of any liquid products, such as ethanol; and part V, gas chromatography (GC, SRI 8610C) using a flame ionization detector (FID). In addition, a branch connection to MS was included to perform temperature-programmed desorption-mass spectrometer (TPD-MS) measurements.

The operation conditions for each part are as follows: For part I, the max flow speed for H_2, CO_2, and He is 10 ml/min, 10 ml/min, and 73 ml/min, respectively. For part II, DRIFTS can be operated in the pressure range from 10^{-6} mbar to 10^6 mbar and in the temperature range from room temperature (RT) to 1173 K with an optimized scan speed of 38 scans/min. In addition, the entire DRIFTS part is maintained in N_2 gas flush to eliminate interference from atmospheric H_2O and CO_2 whose vibrational signals are especially IR sensitive. For part III, the MS measurements were performed at pressure below 10^{-5} mbar with a scan speed of 200 ms/amu in a mass range of 0–50. For parts IV and V, the exhaust gas passes through DIW and GC at ambient pressure. The measurement time (retention time) was set as 9 min for GC measurement with an interval time of 4 min between each measurement. Note that a back-pressure regulator has been placed at the exhaust gas line of DRIFTS.

The function of each part is as follows: For part I, a gas flow controller is utilized to precisely control gas flows using digital commands. For part II, DRIFTS scans the surface adsorption species
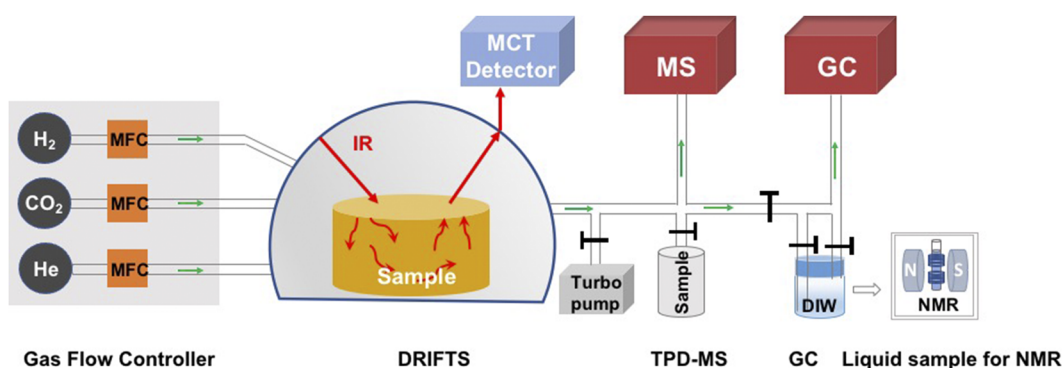
FIG. 1. Schematic of the DRIFTS–MS–GC instrument utilized in this study.

in addition to detecting the gas phase. For part III, MS detects the gas-phase reactants and products. For part IV, DIW collects any liquid products for NMR analysis. For part V, GC detects the gas phase to complement the analysis of gas products that have overlapped signals in MS.

B. Experimental procedures

1. Materials preparation

Fe, Co, Ni, and Cu powders (99%, max. particle size 60 μm, Goodfellow) were used as purchased but compressed into soft pellets of the same size as the DRIFTS chamber (diameter 6 mm and thickness 3.5 mm). Although the DRIFTS normally requires samples to not be pressurized, we observed that most of the intensity of the infrared (IR) signal was maintained over the soft pellet surface compared to the powder surface. Moreover, pellet samples exhibit two important advantages compared to the powder samples. First, pellet samples have little problem of sample loss due to gas flow or pumping, which is particularly important for nanomaterials. Second, pellets have better thermal conductivity during the heating experiment.

LaNi$_4$Cu was synthesized through arc melting of La, Ni, and Cu metals under an Ar atmosphere. The details can be found in our previous work.[36] The LaNi$_4$Cu alloy was activated in pure H$_2$ gas at a pressure of 20 bars. The bulk alloy became a powder after H$_2$ activation. After releasing the high-pressure H$_2$, the sample was transferred to the DRIFTS chamber via an operation in the Ar gas-filled glovebox.

Co—CoO was synthesized by reducing Co$_3$O$_4$ nanoparticles in an H$_2$/He flow [(6 ml/min)/(4 ml/min)] in the DRIFTS chamber at 523 K for 4 h with a heating rate of 2 K/min. Afterward, the sample was cooled down in the same H$_2$/He flow. The Co$_3$O$_4$ nanoparticles were prepared by the calcination of Co(NO$_3$)$_2 \cdot$ 6H$_2$O (Sigma-Aldrich, 99%). The calcination program was set to 573 K for 12 h and continuing heating to 673 K for 2 h using a heating rate of 2 K/min.

2. Reaction conditions

a. CO$_2$ adsorption and hydrogenation reactions on pristine metals. The pristine Fe, Co, Ni, and Cu metal samples were loaded

in the DRIFTS chamber and then evacuated to high vacuum at RT. The IR spectrum background was recorded on the metal surface at this high vacuum. The CO$_2$ adsorption experiment was executed by filling this evacuated DRIFTS chamber with pure CO$_2$ gas of 1 bar. Afterward, the samples were heated from RT to 773 K with a heating rate of 5 K/min. The spectra were recorded at every 50 K. The CO$_2$ hydrogenation reactions on Fe, Co, Ni, and Cu metals were also performed in the closed chamber condition. Again, the chamber was first pumped to high vacuum at RT. Afterward, the samples were heated to 473 K in the vacuum, and the IR backgrounds were recorded. Then, 200 mbar CO$_2$ and 800 mbar H$_2$ were filled in the chamber. The spectra were recorded every half an hour.

b. CO$_2$ hydrogenation reaction on metal hydride. The LaNi$_4$Cu alloy sample was loaded into the DRIFTS chamber through air-free operation. The chamber was then pumped to high vacuum at RT. The IR background was recorded later on. Then, 200 mbar CO$_2$ and 800 mbar H$_2$ were filled in the chamber. The sample was heated from RT to 723 K with a heating rate of 2 K/min, and the spectra were scanned continuously every 10 K.

c. CO$_2$ hydrogenation on metal–metal oxide. The CO$_2$ hydrogenation reaction on the Co—CoO catalyst surface was carried out under continuous gas flow conditions. After the Co—CoO catalyst was synthesized in the DRIFTS chamber, the IR background was recorded. Then, CO$_2$ at 1.5 ml/min, H$_2$ at 6 ml/min, and He at 2.5 ml/min were allowed to flow through the whole DRIFTS–MS–GC system. Heating from RT to 623 K with a ramp of 2 K/min was applied to the sample. The IR spectra were recorded every 20 K. The MS measured the mass range of 0 amu–50 amu with a rate of 0.2 s/amu. The GC took 9 min to obtain each spectrum with a cooling interval of 4 min between each measurement.

C. Determinations of rate constant and activation energy

The main reaction of CO$_2$ hydrogenation is

$$CO_2 + 4H_2 \leftrightarrow CH_4 + 2H_2O. \tag{1}$$
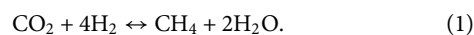
At low conversion, the reverse reaction can be neglected. Hence, the reaction kinetics can be simplified as

$$\frac{d[CH_4]}{dt} = -k[CO_2]^m[H_2]^n, \qquad (2)$$

where $[CH_4]$, $[CO_2]$, and $[H_2]$ are the concentrations of CH_4, CO_2, and H_2, respectively, at reaction time t, with units of mol/l; k is the rate constant; and m and n are the reaction orders of CO_2 and H_2, respectively.

According to the stoichiometry, $[H_2]$ is fourfold $[CO_2]$. As we kept the gas feed of H_2 and CO_2 at a ratio of 4:1, $[H_2]$ can be replaced by $4 \cdot [CO_2]$. As for the reaction orders, the reaction order of CO_2 is reported to be less than 0.4 and that of H_2 is less than 0.9 at reaction temperatures lower than 523 K.[38–41] Therefore, we assume the overall reaction order is 1. Thence, the reaction kinetics is further simplified as

$$\frac{d[CH_4]}{dt} = -k'[CO_2]^{m+n}, \qquad (3)$$

where $m + n$ is 1 and k' is $4^n \cdot k$.

Therefore, the kinetic parameters can be derived by the variation of CH_4 and CO_2 over the reaction.

Note that Eq. (3) is the reaction rate of the overall reaction, which is from the beginning of dose of CO_2 to the end of the product of CH_4. Therefore, the intermediate steps between CO_2 and CH_4, i.e., $CO_2 \rightarrow$ surface reactive species $\rightarrow CH_4$, are incorporated. However, if the feeding ratio of H_2/CO_2 is not 4 (nonstoichiometric), this simplification of Eq. (3) could not be used. Instead, $[H_2]$, $[CO_2]$, m, and n have to be quantified independently, and their real values have to be all used as described in Eq. (2).

1. Determination of gas concentrations

We used two models of CO_2 hydrogenation reactions: constant volume without gas flow for the pristine and alloyed metals, and constant pressure with gas flow for the metal–metal oxide. Therefore, we used two different evaluation methods. For the constant volume reaction, the pressure in the DRIFTS reaction chamber could be easily tracked by the pressure sensor, which is connected right before the reaction chamber. The quantity of each gas component is then calculated from the partial pressure. This calculation method was used for calculating the CH_4 yield over the four pure metals and the kinetic constant and activation energy over $LaNi_5Cu$.

For the constant pressure (flow gas) reaction, the quantification is more challenging. The molar quantities of H_2, CO_2, CH_4, and He gases were determined using MS signals with m/z at 2, 44, 15, and 4, respectively. We mixed $H_2/CO_2/He$ or $CH_4/CO_2/He$ gases at different concentrations to obtain the correlation between the concentration and the MS signal. He gas not only acted as a carrier gas but also as the reference intensity of the MS signal. Herein, for H_2, CO_2, and CH_4 gases, we obtained

$$\frac{f(H_2)}{f(He)} = (3.98 \pm 0.18) \cdot \frac{I(H_2)}{I(He)}, \qquad (4)$$

$$\frac{f(CO_2)}{f(He)} = (2.57 \pm 0.04) \cdot \frac{I(CO_2)}{I(He)}, \qquad (5)$$

$$\frac{f(CH_4)}{f(He)} = (2.50 \pm 0.17) \cdot \frac{I(CH_4)}{I(He)}, \qquad (6)$$

where $f(H_2)$, $f(CO_2)$, $f(CH_4)$, and $f(He)$ (ml/min) are the flow rates of H_2, CO_2, CH_4, and He gases, respectively, and $I(H_2)$, $I(CO_2)$, $I(CH_4)$, and $I(He)$ are the MS signal intensities with m/z at 2, 44, 15, and 2, respectively.

Combining Eqs. (4)–(6), we can finally obtain the transient CO_2 and CH_4 molar numbers,

$$n(CO_2) = \frac{f(CO_2)}{24.5}, \qquad (7)$$

$$n(CH_4) = \frac{f(CH_4)}{24.5}, \qquad (8)$$

where 24.5 ml/mol is the molar volume of the ideal gas at 298 K.

Equation (3) for calculating the kinetic constant can now be expressed as

$$\frac{dn(CH_4)}{dt} = -k'n(CO_2). \qquad (9)$$

The reaction time t is the gas passing time through the sample, which is calculated as

$$t = \frac{V_{sample}}{f_{total}}, \qquad (10)$$

where V_{sample} is the sample volume calculated from the size of the sample pellet and f_{total} is the total flow of the mixed gases, which is 10 ml/min.

2. Determination of activation energy (E_a)

The correlation between k and E_a is determined using the Arrhenius equation,

$$\ln k = \ln A - \frac{E_a}{R} \cdot \frac{1}{T}, \qquad (11)$$

where A is the pre-exponential factor, R is the gas constant, and T is reaction temperature.

Replacing k by k', we obtain

$$\ln k' = \ln A' - \frac{E_a}{R} \cdot \frac{1}{T}, \qquad (12)$$

where the new pre-exponential factor A' is $4^n \cdot A$.

III. RESULTS AND DISCUSSIONS

A. CO₂ adsorption and hydrogenation reactions on the pristine metal surfaces

CO_2 adsorption on the pristine Fe, Co, Ni, and Cu metal surfaces showed only gaseous CO_2 in the IR spectra with asymmetric stretching vibrations centered at 2349 cm^{-1} (not shown). The derivative species, such as non-dissociated product carbonate and dissociated product CO^*, were missing, indicating that CO_2 interacts very weakly on these pristine metal surfaces at RT. This is consistent with the reported low CO_2 binding energies (less than 40 kJ/mol) and with the desorption temperatures lower than RT on the single crystalline metal surfaces.[42,43] To examine whether CO_2 molecules interacted stronger with the pure metal surfaces when

increasing the temperature, we heated the surfaces up to 773 K. As shown in Fig. 2(a), CO gas, with rotational–vibrational modes in the range from 2230 cm^{-1} to 2030 cm^{-1}, was produced on the Fe surface at 673 K. Very low IR intensities of CO gas were also recorded on the Co and Ni surfaces at 673 K. However, no products were detected on the Cu surface over the entire temperature range. Note that the small peak at 2070 cm^{-1} represents the rotational bands of CO_2 gas.[44] Therefore, CO_2 gas interacts with pure Fe, Co, and Ni surfaces at high temperatures by dissociation into CO gas. Fe is the most active metal for the CO_2 dissociation reaction, whereas Cu is not active in the CO_2 adsorption reaction.

CO_2 hydrogenation was subsequently investigated on these four pure metals. This reaction primarily produces CH_4, which is known as the Sabatier reaction. The CH_4 yields at 473 K as a function of reaction time are shown in Fig. 2(b). The highest CH_4 yield occurred on the Co surface and second highest on the Ni surface. After 10 h of reaction, the CH_4 yield on the Co surface was sevenfold higher than that on the Ni surface. No CH_4 was produced on the Fe and Cu surfaces in these conditions. Therefore, Co is the most reactive metal for the CO_2 methanation reaction, and Ni is the second most reactive. This is in line with the previous results from our group.[21] These results suggest that Co is the most promising catalyst for the efficient CO_2 conversion into synthetic methane. This inspires us to design Co-based materials for the further study of CO_2 hydrogenation, which is presented in Sec. III C.

B. CO_2 hydrogenation reaction on the metal hydride surface

In our previous study, we observed that adsorbed H_2 is a key component to weaken the C=O bond of CO_2 to form adsorbed formate or carbon monoxide.[45] Hence, we hypothesize that the poor performance of CO_2 hydrogenation observed for Fe, Ni, and Cu may be caused by insufficient H_2 on the surface. For this reason, we used the $LaNi_4Cu$ alloy for CO_2 reduction as this material represents a classic hydrogen storage material.[36,46] As shown by the IR spectra in Fig. 3(a), CO_2 was consumed along with the production of CH_4 and CO gases when elevating the temperature. We integrated
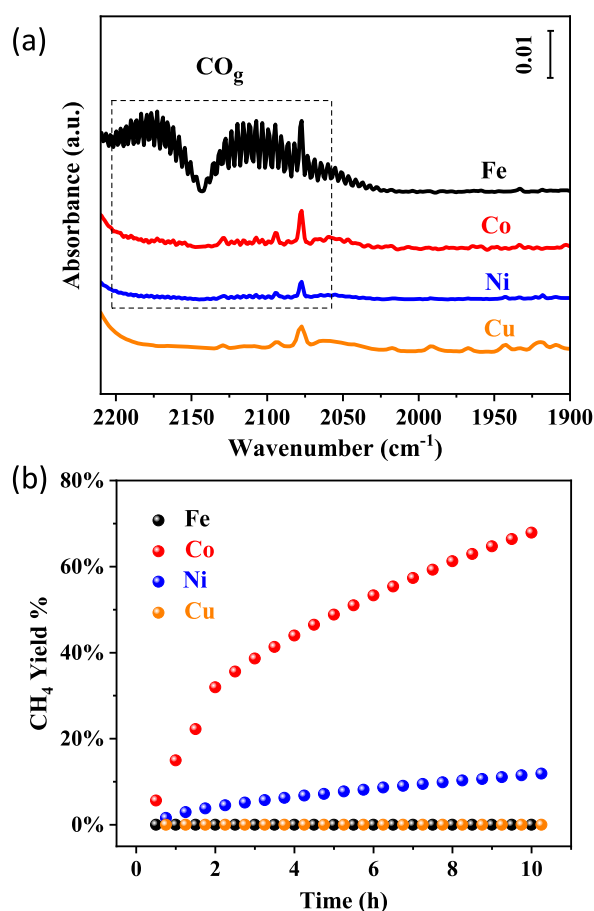

FIG. 2. (a) IR spectra for 1 bar CO_2 adsorption on Fe, Co, Ni, and Cu surfaces at 673 K. (b) CH_4 yields from the CO_2 hydrogenation reactions on the Fe, Co, Ni, and Cu surfaces at 473 K.
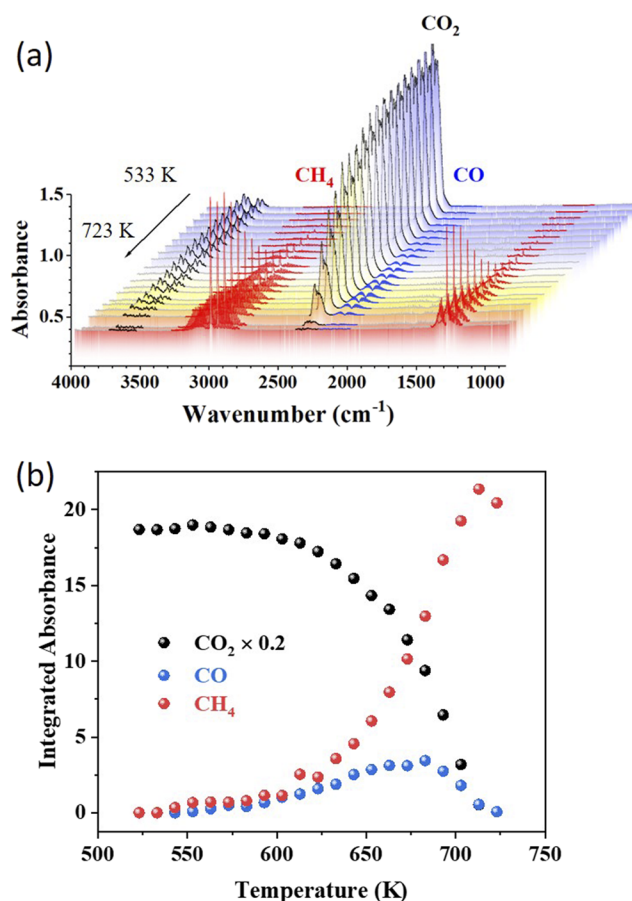

FIG. 3. (a) IR spectra for the CO_2 hydrogenation reaction on the $LaNi_4Cu$ surface at elevating temperatures. (b) The integrated IR absorbance of the gaseous reactant of CO_2 and gaseous products of CO and CH_4. CO_2 intensity was divided by five times.

the absorbance of the reactant and product gases to understand the reaction kinetics. As shown in Fig. 3(b), CH_4 and CO gases emerged above 623 K. CH_4 production continued to increase until 723 K, and CO production continued to increase until 680 K. Above these temperatures, the intensities of these two products started to decrease. Nevertheless, the high onset temperature of the CO_2 hydrogenation reaction signifies that the $LaNi_4Cu$ alloy did not help to lower down the reaction temperature, although the alloy was hydrogenated beforehand. Moreover, as the stored H_2 in the alloy remains stable until 373 K,[46] the high onset temperature for CO_2 hydrogenation invalidated the advantages of H_2 pre-storage. In addition, no adsorbed species were observed from the IR spectra, similar to the cases for pristine metals, making it not possible to explain the intermediate catalyzed steps. Therefore, these pristine and alloyed metals are not suitable for the reaction step study, which is limited by the DRIFTS analysis, and we did not continue to study the reaction over these pure and alloyed metals using the rest of the methods, such as MS, GC, and NMR.

C. CO_2 hydrogenation reaction on the Co−CoO surface

As we found that Co is the most reactive metal for CO_2 methanation among the transition metals tested, and based on the observation that metal oxides provide abundant adsorption sites in our previous study,[45,47,48] we synthesized Co−CoO nanoparticles to investigate the gas, liquid, and surface products under flow gas conditions. The Co−CoO nanoparticles possessed a 20% molar concentration of metallic cobalt, as quantified by the consumed amount of H_2 gas measured using MS.

The CO_2 to CH_4 conversion was analyzed by means of MS. As shown in Fig. 4(a), the CO_2 hydrogenation reaction on this Co−CoO catalyst began at approximately 430 K. The primary and main product was CH_4 with approximately 90% yield. Weak signals of the very small amounts of CO and C_2H_6 detected in MS overlapped with the signal of CO_2 fragments. Therefore, GC was employed to separate these gases. As shown in Fig. 4(b), C_2H_6 and CO production have onset temperatures similar to CH_4 production and show the maximum yield of 0.15% and 0.024%, respectively, both at 543 K. Above 543 K, the observed amount of both C_2H_6 and CO decreased, indicating that high temperatures are not favorable for C_{2+} synthesis and reversed gas shift reactions on Co−CoO. A reason for this phenomenon could be that the intense methanation reaction produced a large amount of H_2O at high conversion of CO_2, as we observed condensed water on the chamber window after a long time reaction at high temperatures. The produced H_2O competitively adsorbs on the surface and inhibits the reaction in the forward direction. Besides the gas products, traces of methanol, ethanol, and acetic acid products were found using NMR, as shown in Fig. 4(c). These latter species could be traced only by means of this analytical method. The overall yield of the non-methane products is less than 0.2%. However, the methods used in the study are able to collect information for all of the products.

After clarified the overall products of CO_2 conversion, we analyzed the intermediates on the surface during the reaction process. We tracked the surface adsorption species using the DRIFTS part. The IR spectral region between 1700 cm^{-1} and 1200 cm^{-1} contains information about the adsorption species [Fig. 5(a)]. These peaks
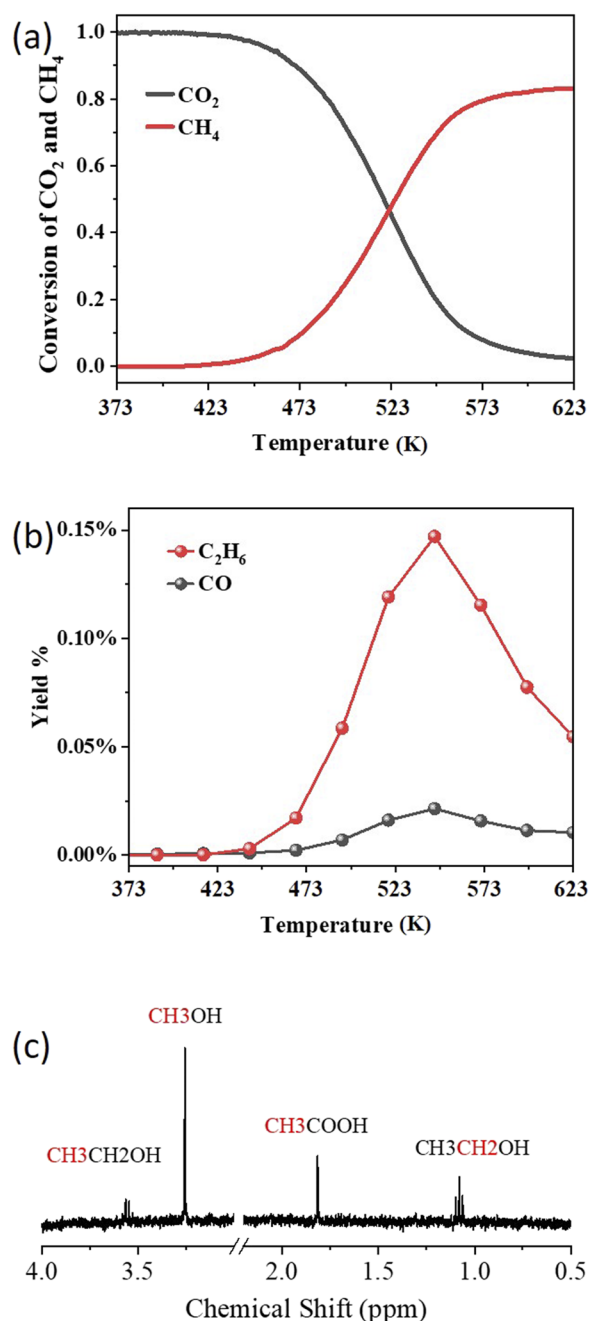

FIG. 4. (a) CO_2 and CH_4 conversion from CO_2 hydrogenation on the Co−CoO surface analyzed using MS data. (b) The calculated yields of C_2H_6 and CO gas products using GC data. (c) Very small quantities of CH_3OH, C_2H_5OH, and CH_3COOH liquid products collected using the inline deionized water and measured using NMR.

formed upon CO_2 and H_2 co-adsorption at RT. A deconvolution using the bi-level evolutionary Gaussian fitting showed the development of the peaks (refer to our previous work for the peak deconvolution, assignment, and identification).[40,47] The peak at 1620 cm^{-1}
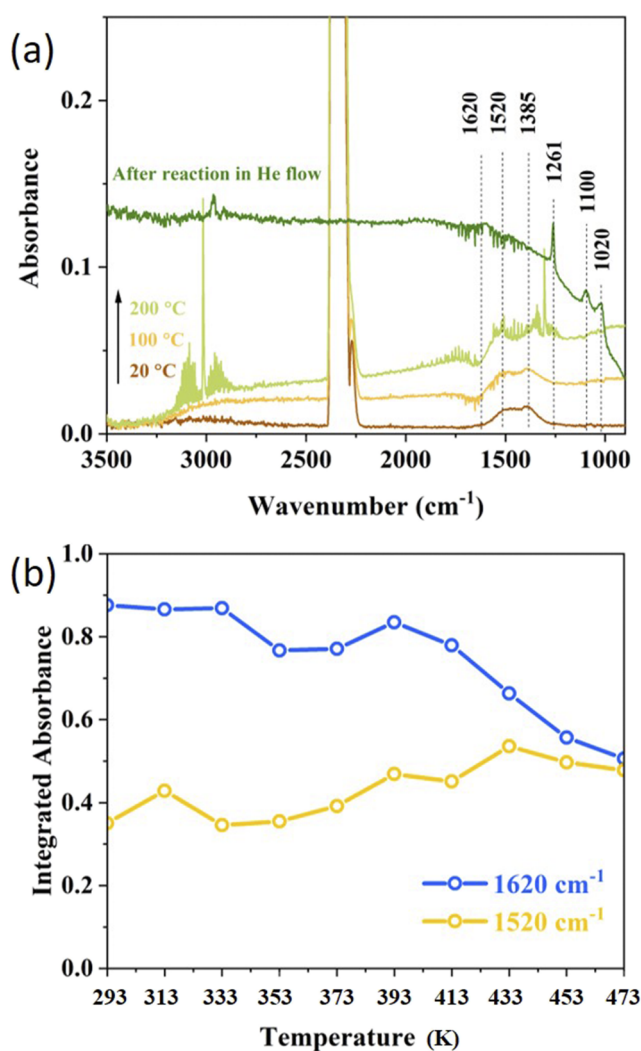
FIG. 5. (a) IR spectra for the CO_2 hydrogenation reaction on the Co—CoO surface. (b) Development of the adsorbed formate and carbonate with IR peaks at 1620 cm^{-1} and 1520 cm^{-1}, respectively.

was ascribed to the O—C—O asymmetric stretching mode of formate on the metal–metal oxide interface, and the wide peak centered at 1520 cm^{-1} was assigned to the adsorbed carbonate ($CO_3^{2-}*$).[45] The wide peak centered at 1385 cm^{-1} was coupled by the C—H bending and O—C—O symmetric stretching of formate.[49–52] As shown in Fig. 5(b), the formate consumed during the reaction, and $CO_3^{2-}*$ did not vary before 473 K. Due to the strong interference of the IR spectra from H_2O, which was formed from the dominant CO_2 methanation reaction, the peaks after 473 K could not be distinguished well. However, after the CO_2 hydrogenation reaction and overnight flashing in He gas, the previously observed formate and carbonate species disappeared, as shown in the top green plot in Fig. 5(a). This suggests that these species are completely consumed above 473 K. However, new peaks at 1261 cm^{-1}, 1100 cm^{-1}, and 1020 cm^{-1} remained on the surface after He flow.

To identify the new peaks, we referred to the NMR results. We separately applied 1 μl of CH_3OH, C_2H_5OH, HCOOH, and CH_3COOH liquids to the resulting Co—CoO surface in the DRIFTS chamber in a glovebox. By comparing the IR peaks of the standard chemicals (spectra not shown), the peak at 1261 cm^{-1} was found to be fitted with the O—H bending mode of C_2H_5OH, the peak at 1100 cm^{-1} overlapped with the C—O stretching of HCOOH and C_2H_5OH, and the peak at 1020 cm^{-1} overlapped with the C—O stretching of CH_3OH and C_2H_5OH.[53] These species may have been retained on the surface after CO_2 reduction. Yet, the retained species could also be strongly bound CO* and bidentate carbonate on the cobalt.[54]

Consequently, the surface analysis provided the information that the formate at the metal–metal oxide interface and carbonate at the metal oxide formed upon CO_2 and H_2 co-adsorption. These two species were the intermediates of CH_4 formation. Some carbon oxides, either alcohol/acid or strongly bound CO*, were retained on the Co—CoO surface as by-products.

Comparing to the invisible surface species on the pristine and alloyed metals, we speculate that the metal surfaces interact with CO_2 molecules weakly in the applied dry gas and clean surface condition, as the observations of CO_2 adsorption and desorption on metal surfaces are in ultrahigh vacuum and at low temperatures (<273 K).[55–57] However, on the oxide surface, CO_2 adsorption and desorption are usually above room temperature.[42,58] Therefore, the physical properties of the material surface determine the CO_2 adsorption behavior and result in the invisible adsorbed species on the metal and visible adsorbed species on the metal oxide or the interface of the metal and metal oxide. Metal oxide is essentially important for the mechanism study of the surface reactions.

D. Kinetic comparison of the CO_2 methanation reaction on the pristine and alloyed metals, and the Co—CoO surface

As a final example of the capabilities of the instrumental setup here developed, we calculated the kinetics of CO_2 methanation on the three types of catalysts studied to compare the activities of these catalysts. We calculated the kinetic constants at 473 K using Eq. (9). As shown in Fig. 6 (left axis), Co—CoO exhibits tremendously higher kinetic constant than the pristine Co metal; Co metal possesses tenfold higher kinetics than Ni; and $LaNi_4Cu$ is not reactive at 473 K. These explained the high activity of the Co—CoO sample.

The activation energies (E_a) of CO_2 methanation were calculated using Eq. (12) for Co—CoO and $LaNi_4Cu$ samples at their low CO_2 conversions of 2%–40%. These low conversions related to temperature ranges of 440 K–510 K for Co—CoO and 583 K–663 K for $LaNi_4Cu$. The values of E_a on Co and Ni were taken from a previous work of our group.[18] The results are shown in Fig. 6 (right axis). Co—CoO has higher activation energy than Co and Ni, indicating that the kinetic constant changes faster with temperature on Co—CoO than on Co and Ni. This is in line with the observations in Figs. 2(b) and 4(a). $LaNi_4Cu$ has the highest activation energy, which is consistent with its less active at low temperatures and reflects the reaction rate changing fast at high temperatures. These are in line with the observations in Fig. 3. These results emphasize the importance of the presence of the metal oxide phase in the
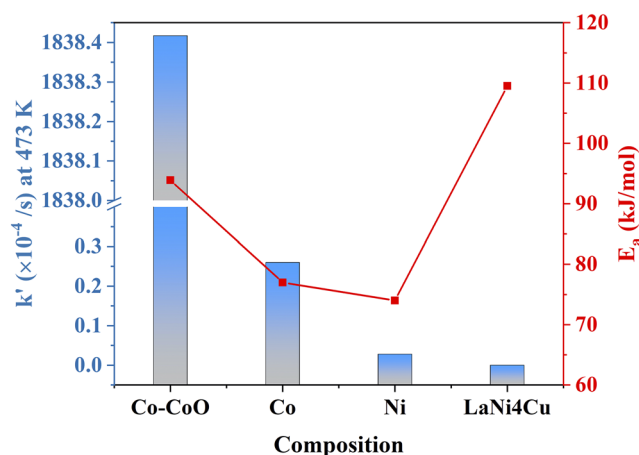
FIG. 6. Reaction rate constants k' at 473 K (left axis) and activation energies E_a of CO_2 methanation (right axis). Activation energies of CO_2 methanation on Co and Ni were taken from Ref. 21.

enhancement of the activity of the catalyst in the CO_2 methanation reaction.

IV. CONCLUSIONS

We built an inline DRIFTS–MS–GC apparatus to perform an *operando* study of the heterogeneously catalyzed CO_2 hydrogenation reaction. Pristine metals, metal hydride alloys, and metal–metal oxide materials were used as example materials to show the potential of the system and the related analytic methods, including the calculation of the kinetic parameters of the reaction and the resolving of the complicated adsorption species. The results verified the reliability of the combined system and the sensitivity of this apparatus for the simultaneous investigation of the gas, liquid, and surface products of CO_2 adsorption and hydrogenation reactions. Importantly, the observation of the adsorbed species on the catalyst surface requires the presence of a metal oxide phase in the catalyst. No adsorbed species but only the gas phase was found on the purely metallic surfaces, such as pristine and alloyed metals.

In addition to the development of this special instrument and the correspondingly analytic method, this study shows the systematic understanding of the fundamental differences in the interaction of CO_2 with metals and provides instructions of synthesizing a highly active and efficient catalyst. Co is the most active metal to hydrogenate CO_2 to CH_4, while Fe is the most active to dissociate CO_2 to CO gas. Pre-stored H_2 in metal hydride alloys does not assist the CO_2 hydrogenation. However, metal oxides mixed with metal facilitate the CO_2 hydrogenation due to the adsorption of CO_2 at the metal oxide surface and the metal/metal oxide interface. As a result, the activity in the CO_2 methanation follows the order of Co—CoO > Co > Ni > LaNi$_4$Cu. This enlightens the importance of the metal oxide phase in the design of the efficient catalyst to achieve high activity in CO_2 methanation.

Overall, the coupling of different analytic techniques in a single experimental unit is therefore essential for the advancement of science in this complex field, enabling the contemporaneous understanding of different effects, which could not be revealed by means of the single individual tools.

DATA AVAILABILITY

The data that support the findings of this study are available from the corresponding author upon reasonable request.

REFERENCES

[1] N. S. Lewis and D. G. Nocera, Proc. Natl. Acad. Sci. U. S. A. **103**, 15729 (2006).
[2] M. Aresta and A. Dibenedetto, Catal. Today **98**, 455 (2004).
[3] A. Züttel, P. Mauron, S. Kato, E. Callini, M. Holzer, and J. Huang, CHIMIA Int. J. Chem. **69**, 264 (2015).
[4] S. Gao, Y. Lin, X. Jiao, Y. Sun, Q. Luo, W. Zhang, D. Li, J. Yang, and Y. Xie, Nature **529**, 68 (2016).
[5] W.-H. Wang, Y. Himeda, J. T. Muckerman, G. F. Manbeck, and E. Fujita, Chem. Rev. **115**, 12936 (2015).
[6] R. W. Dorner, D. R. Hardy, F. W. Williams, and H. D. Willauer, Energy Environ. Sci. **3**, 884 (2010).
[7] W. L. Vrijburg, E. Moioli, W. Chen, M. Zhang, B. J. P. Terlingen, B. Zijlstra, I. A. W. Filot, A. Züttel, E. A. Pidko, and E. J. M. Hensen, ACS Catal. **9**, 7823 (2019).
[8] R. Mutschler, E. Moioli, K. Zhao, L. Lombardo, E. Oveisi, A. Porta, L. Falbo, C. G. Visconti, L. Lietti, and A. Züttel, ACS Catal. **10**, 1721 (2020).
[9] E. Moioli, N. Gallandat, and A. Züttel, Chem. Eng. J. **375**, 121954 (2019).
[10] E. Moioli, R. Mutschler, and A. Züttel, Renewable Sustainable Energy Rev. **107**, 497 (2019).
[11] E. Moioli and A. Züttel, Sustainable Energy Fuels **4**, 1396 (2020).
[12] F. Marques Mota and D. H. Kim, Chem. Soc. Rev. **48**, 205 (2019).
[13] W. Li, H. Wang, X. Jiang, J. Zhu, Z. Liu, X. Guo, and C. Song, RSC Adv. **8**, 7651 (2018).
[14] E. Moioli, N. Gallandat, and A. Züttel, React. Chem. Eng. **4**, 100 (2018).
[15] M. Jacquemin, A. Beuls, and P. Ruiz, Catal. Today **157**, 462 (2010).
[16] J. Szanyi and J. H. Kwak, Phys. Chem. Chem. Phys. **16**, 15117 (2014).
[17] M. Che, Catal. Today **218-219**, 162 (2013).
[18] J. H. Kwak, L. Kovarik, and J. Szanyi, ACS Catal. **3**, 2449 (2013).
[19] J. Lahtinen, T. Anraku, and G. A. Somorjai, Catal. Lett. **25**, 241 (1994).
[20] G. D. Weatherbee and C. H. Bartholomew, J. Catal. **68**, 67 (1981).
[21] R. Mutschler, E. Moioli, W. Luo, N. Gallandat, and A. Züttel, J. Catal. **366**, 139 (2018).
[22] K. O. Xavier, R. Sreekala, K. K. A. Rashid, K. K. M. Yusuff, and B. Sen, Catal. Today **49**, 17 (1999).
[23] B. Mutz, M. Belimov, W. Wang, P. Sprenger, M.-A. Serrer, D. Wang, P. Pfeifer, W. Kleist, and J.-D. Grunwaldt, ACS Catal. **7**, 6802 (2017).
[24] S. Zhang, L. Nguyen, J.-X. Liang, J. Shan, J. Liu, A. I. Frenkel, A. Patlolla, W. Huang, J. Li, and F. Tao, Nat. Commun. **6**, 7938 (2015).
[25] J. He, N. J. J. Johnson, A. Huang, and C. P. Berlinguette, ChemSusChem **11**, 48 (2018).

[26] M. Schubert, S. Pokhrel, A. Thomé, V. Zielasek, T. M. Gesing, F. Roessner, L. Mädler, and M. Bäumer, Catal. Sci. Technol. **6**, 7449 (2016).

[27] S. Wohlrab, D. Ehrlich, J. Wambach, H. Kuhlenbeck, and H.-J. Freund, Surf. Sci. **220**, 243 (1989).

[28] C. Vogt, E. Groeneveld, G. Kamsma, M. Nachtegaal, L. Lu, C. J. Kiely, P. H. Berben, F. Meirer, and B. M. Weckhuysen, Nat. Catal. **1**, 127 (2018).

[29] V. Iablokov, S. K. Beaumont, S. Alayoglu, V. V. Pushkarev, C. Specht, J. Gao, A. P. Alivisatos, N. Kruse, and G. A. Somorjai, Nano Lett. **12**, 3091 (2012).

[30] F. C. Meunier, Chem. Soc. Rev. **39**, 4602 (2010).

[31] T. Franken, J. Terreni, A. Borgschulte, and A. Heel, J. Catal. **382**, 385 (2020).

[32] N. Boreriboon, X. Jiang, C. Song, and P. Prasassarakich, Top. Catal. **61**, 1551 (2018).

[33] L. Wang, W. Zhang, X. Zheng, Y. Chen, W. Wu, J. Qiu, X. Zhao, X. Zhao, Y. Dai, and J. Zeng, Nat. Energy **2**, 869 (2017).

[34] G. D. Weatherbee and C. H. Bartholomew, J. Catal. **87**, 352 (1984).

[35] C. Liu, T. R. Cundari, and A. K. Wilson, J. Phys. Chem. C **116**, 5681 (2012).

[36] M. Spodaryk, N. Gasilova, and A. Züttel, J. Alloys Compd. **775**, 175 (2019).

[37] A. Boffa, C. Lin, A. T. Bell, and G. A. Somorjai, J. Catal. **149**, 149 (1994).

[38] M. S. Duyar, A. Ramachandran, C. Wang, and R. J. Farrauto, J. CO2 Util. **12**, 27 (2015).

[39] G. D. Weatherbee and C. H. Bartholomew, J. Catal. **77**, 460 (1982).

[40] A. Karelovic and P. Ruiz, ACS Catal. **3**, 2799 (2013).

[41] G. Garbarino, D. Bellotti, E. Finocchio, L. Magistri, and G. Busca, Catal. Today **277**, 21 (2016).

[42] U. Burghaus, Prog. Surf. Sci. **89**, 161 (2014).

[43] B. Bartos, H.-J. Freund, H. Kuhlenbeck, M. Neumann, H. Lindner, and K. Müller, Surf. Sci. **179**, 59 (1987).

[44] C. P. Rinsland, D. C. Benner, and V. M. Devi, Appl. Opt. **25**, 1204 (1986).

[45] K. Zhao, L. Wang, M. Calizzi, E. Moioli, and A. Züttel, J. Phys. Chem. C **122**, 20888 (2018).

[46] A. Züttel, Mater. Today **6**, 24 (2003).

[47] K. Zhao, L. Wang, E. Moioli, M. Calizzi, and A. Züttel, J. Phys. Chem. C **123**, 8785 (2019).

[48] K. Zhao, M. Calizzi, E. Moioli, M. Li, A. Borsay, L. Lombardo, R. Mutschler, W. Luo, and A. Züttel, J. Energy Chem. **53**, 241 (2021).

[49] G. Busca, J. Lamotte, J. C. Lavalley, and V. Lorenzelli, J. Am. Chem. Soc. **109**, 5197 (1987).

[50] K. Ito and H. J. Bernstein, Can. J. Chem. **34**, 170 (1956).

[51] H. R. Zelsmann, Y. Marechal, A. Chosson, and P. Faure, J. Mol. Struct. **29**, 357 (1975).

[52] Y. T. Chang, Y. Yamaguchi, W. H. Miller, and H. F. Schaefer, J. Am. Chem. Soc. **109**, 7245 (1987).

[53] E. K. Plyler, J. Res. Natl. Bur. Stand. **48**, 281 (1952).

[54] J. Paul and F. M. Hoffmann, Catal. Lett. **1**, 445 (1988).

[55] X. Ding, L. De Rogatis, E. Vesselli, A. Baraldi, G. Comelli, R. Rosei, L. Savio, L. Vattuone, M. Rocca, P. Fornasiero, F. Ancilotto, A. Baldereschi, and M. Peressi, Phys. Rev. B **76**, 195425 (2007).

[56] H.-J. Freund and R. P. Messmer, Surf. Sci. **172**, 1 (1986).

[57] H.-J. Freund and M. W. Roberts, Surf. Sci. Rep. **25**, 225 (1996).

[58] U. Burghaus, *New and Future Developments in Catalysis* (Elsevier, Amsterdam, 2013), pp. 27–47.